NUMERICAL SIMULATION OF THE GENERATION OF MESOSCALE CONVECTIVE SYSTEMS IN LARGE-SCALE ENVIRONMENT

Xia Daqing (夏大庆) and *Zheng Liangjie* (郑良杰)

Institute of Meteorological Research, Headquarters of the General Staff, PLA, Beijing

Received November 20, 1984

ABSTRACT

The generation of mesoscale convective systems is simulated by a 7-level primitive equation model. The large-scale parts of observed data at 1200 Z June 11, 1983, which are obtained by low-pass filter, are used as the initial data. The results show that the generation of mesoscale convective systems can be simulated from fields of meteorological variables on the large-scale background. When the low-level southwest jet stream is very moist, mesoscale convective systems can develop ahead of the wind speed maximum in the warm sector of Jiang-Huai (Changjiang-Huaihe Rivers) cyclone, where the potential stability tends to remain negative. Furthermore, they are similar to the mesoscale convective complex (MCC), which appears frequently in the central part of the United States during the warm season (March to September), in dynamical and thermal structure, distribution of precipitation and the process of generation and development.

I. INTRODUCTION

In recent years, a kind of intermediate-scale convective cloud cluster with horizontal scale up to 1000 km has been found from enhanced infrared geosynchronous satellite images and radar observations. They are frequently found in South, East, North and even Northwest China in summer as well as the central part of the United States. The mesoscale convective system associated with the cloud cluster has a long-life cycle accompanied by strong winds, tornadoes, hailstorms and heavy rains over a broad area, causing floods. Maddox[1] designated this kind of mesoscale convective systems as mesoscale convective complex (MCC) and provided a definition of MCC according to the features of cloud clusters observed from enhanced infrared satellite images. Recently, Maddox[2] revealed their dynamical and thermodynamical features on the basis of a composite analysis of 10 cases of MCC.

In China, Tao et al.[3] have indicated that, during the Changjiang Valley meiyu season, the meso- or intermediate-scale convective cloud clusters emerge frequently at the western end of the stationary frontal shear-line, where the active south-westerly monsoon cloud systems encounter the middle latitude short wave trough moving out of the Tibetan Plateau. This is confirmed by our survey of the enhanced satellite images of June and July from 1980 to 1983. The mesoscale convective systems corresponding to these cloud clusters, however, are difficult to discover from conventional synoptic charts.

The potential instability is an important energy source supporting the violent development of mesoscale convective systems. The aim of our experiment is to simulate, from the

synoptic-scale background, the formation of mesoscale convective systems by changing the distribution of potential instability, and to analyse its dynamical and thermodynamical structures.

II. BRIEF DESCRIPTION OF THE MODEL

A dual grid multi-level primitive equation model[4] with the generalized $\sigma=\left(\frac{p-p_\tau}{p_s-p_\tau}\right)$ coordinate is used in our experiment. The basic equations are:

$$\frac{\partial}{\partial t}\left(\frac{\pi u}{m}\right)=-m\left[\frac{\partial}{\partial x}\left(\frac{\pi u}{m}u\right)+\frac{\partial}{\partial y}\left(\frac{\pi v}{m}u\right)\right]-\frac{\partial}{\partial\sigma}\left(\frac{\pi\dot{\sigma}}{m}u\right)+f\frac{\pi v}{m}$$
$$-\pi\left(\frac{\partial\varphi}{\partial x}+\frac{RT\sigma}{\sigma\pi+p_\tau}\frac{\partial\pi}{\partial x}\right)-\frac{g}{m}\frac{\partial\tau_x}{\partial\sigma}+\frac{K}{m}\nabla\cdot(\pi\nabla u), \tag{1}$$

$$\frac{\partial}{\partial t}\left(\frac{\pi v}{m}\right)=-m\left[\frac{\partial}{\partial x}\left(\frac{\pi u}{m}v\right)+\frac{\partial}{\partial y}\left(\frac{\pi v}{m}v\right)\right]-\frac{\partial}{\partial\sigma}\left(\frac{\pi\dot{\sigma}}{m}v\right)-f\frac{\pi u}{m}$$
$$-\pi\left(\frac{\partial\varphi}{\partial y}+\frac{RT\sigma}{\sigma\pi+p_\tau}\frac{\partial\pi}{\partial y}\right)-\frac{g}{m}\frac{\partial\tau_y}{\partial\sigma}+\frac{K}{m}\nabla\cdot(\pi\nabla v), \tag{2}$$

$$\frac{\partial}{\partial t}\left(\frac{\pi T}{m}\right)=-m\left[\frac{\partial}{\partial x}\left(\frac{\pi u}{m}T\right)+\frac{\partial}{\partial y}\left(\frac{\pi v}{m}T\right)\right]-\frac{\partial}{\partial\sigma}\left(\frac{\pi\dot{\sigma}}{m}T\right)+\frac{\pi RT}{C_p(\sigma\pi+p_\tau)}$$
$$\times\left[\frac{\pi\dot{\sigma}}{m}+\sigma\frac{\partial}{\partial t}\left(\frac{\pi}{m}\right)+\sigma\left(u\frac{\partial\pi}{\partial x}+v\frac{\partial\pi}{\partial y}\right)\right]-\frac{g}{mC_p}\frac{\partial H}{\partial\sigma}$$
$$+\frac{K}{m}\nabla\cdot(\pi\nabla T)+\frac{\pi L}{mC_p}(\dot{p}_L+\dot{p}_C), \tag{3}$$

$$\frac{\partial}{\partial t}\left(\frac{\pi q}{m}\right)=-m\left[\frac{\partial}{\partial x}\left(\frac{\pi u}{m}q\right)+\frac{\partial}{\partial y}\left(\frac{\pi v}{m}q\right)\right]-\frac{\partial}{\partial\sigma}\left(\frac{\pi\dot{\sigma}}{m}q\right)$$
$$-\frac{g}{m}\frac{\partial E}{\partial\sigma}+\frac{K}{m}\nabla\cdot(\pi\nabla q)-\frac{\pi}{m}(\dot{p}_L+\dot{p}_C), \tag{4}$$

$$\frac{\partial}{\partial t}\left(\frac{\pi}{m}\right)=-\int_0^1 m\left[\frac{\partial}{\partial x}\left(\frac{\pi u}{m}\right)+\frac{\partial}{\partial y}\left(\frac{\pi v}{m}\right)\right]d\sigma, \tag{5}$$

$$\frac{\pi\dot{\sigma}}{m}=-\int_0^\sigma m\left[\frac{\partial}{\partial x}\left(\frac{\pi u}{m}\right)+\frac{\partial}{\partial y}\left(\frac{\pi v}{m}\right)\right]d\sigma-\sigma\frac{\partial}{\partial t}\left(\frac{\pi}{m}\right), \tag{6}$$

$$\frac{\partial}{\partial\sigma}\left(\frac{\partial\varphi}{\partial t}\right)=-\frac{R}{\sigma\pi+p_\tau}\left[\pi\frac{\partial T}{\partial t}+\frac{p_\tau T}{\sigma\pi+p_\tau}\frac{\partial\pi}{\partial t}\right], \tag{7}$$

$$\alpha=\frac{RT}{\sigma\pi+p_\tau}, \tag{8}$$

where $\pi=p_s-p_\tau$, p_s is the surface pressure, p_τ ($=100$ hPa) is the pressure at the top of the model atmosphere, K the coefficient of horizontal diffusion, τ, H and E are vertical turbulent fluxes of momentum, sensible heat and water vapor respectively. $\dot{p}_L$ and $\dot{p}_C$ are rates of condensation on large-scale and convective scale. Others are usual symbols in meteorology.

In our experiment, a non-nested mesh is used. 7 levels are taken in the vertical direction. The mesh consists of 21×21 grid points. The spacing is 100 km between grid points and the time step is 3 min. The conservative scheme is employed for spatial finite differences and Euler backward differences for time difference. Davies boundary condition[5] is taken at lateral boundaries of the finite area. In the scheme in which water vapor is incorporated, the large-scale precipitation is evaluated by the method of saturated condensation and the convective precipitation is adjusted with a procedure similar to that of Gadd[6].

III. INITIAL DATA AND EXPERIMENTAL SCHEME

The field of observed geopotential heights at 1200 Z June 11, 1983 when the cyclone over the Changjing-Huaihe Valley in its developing stage, is processed by low-pass filter[7], so the initial field of geopotential heights is obtained from the large-scale background. Then, the initial temperatures are derived from the hydrostatic equation and winds from the balance equation in σ-coordinate. The numerical experiments are carried out in three schemes as follows:

Scheme 1: No effect of water vapor is incorporated in the model.

Scheme 2: As initial data, observed water vapor values are incorporated.

Scheme 3: An artificially modified water vapor field is incorporated.

Fig. 1 is the surface pressure field after low-pass filtering. It is seen that the inversed pressure trough, which is the main feature in the large-scale background, remains in the region of integration. A low-level southwesterly jet stream with a maximum speed of 16 m/s lies to the right of the trough on the 700 hPa surface.

Usually, potential instability is an important condition for the development of mesoscale systems. Diagnostic analysis, however, shows that heavy rain often takes place downstream of the most unstable area, where the convergence of water vapor is strongest. In general, this condition is easily met ahead of the warm and moist low-level jet stream. In order to stress the effect of potential instability, the air below $\sigma=9/14$ (i.e., about 680 hPa) in Scheme 3 is modified to become saturated in such an area where the initial wind speed in the low-level jet stream on the 700 hPa surface is higher than 15 m/s (the shaded area in Fig. 1). Such modification is carried out once per hour during the integration process. In this way, the shaded area in Fig. 1 may act as a source of water vapor or unstable energy.

To examine the tendency of variation of potential stability during the integration process, we introduce the tendency equation of potential stability

$$\frac{\partial}{\partial t}\left(-\frac{\partial E_\sigma}{\partial\sigma}\right)=C_p\frac{\partial}{\partial\sigma}\left(\mathbf{V}\cdot\nabla T+\dot\sigma\frac{\partial T}{\partial\sigma}\right)+\frac{\partial}{\partial\sigma}\left(\mathbf{V}\cdot\nabla\varphi+\dot\sigma\frac{\partial\varphi}{\partial\sigma}\right)$$

$$+L\frac{\partial}{\partial\sigma}\left(\mathbf{V}\cdot\nabla q+\dot\sigma\frac{\partial q}{\partial\sigma}\right), \tag{9}$$

where $E_\sigma=C_pT+gz+Lq$ is the static energy. It is seen from the equation that the tendency of potential stability depends on the interaction between the fields of temperature, pressure, water vapor and motion. Computation in Scheme 3 with artificially modified water vapor distribution shows that the tendency of potential stability in the lower layers is essentially determined by the vertical distribution of water vapor advection.

The distribution of tendency of potential stability for Scheme 3 on the $\sigma=7/14$ surface at the end of the first hour integration is given in Fig. 2. Three negative and one positive

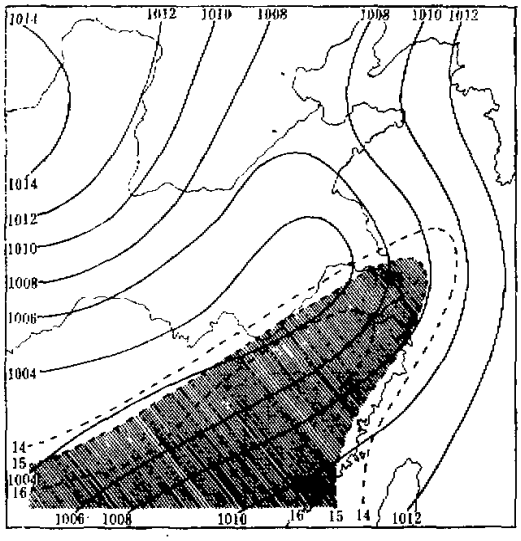

Fig. 1. The large-scale background of surface pressure at 1200 Z June 11, 1983. Solid lines are isobars (in hPa) and dashed lines are isotaches (in m/s). The shaded area denotes the region where the air is assumed to be saturated with water vapor.

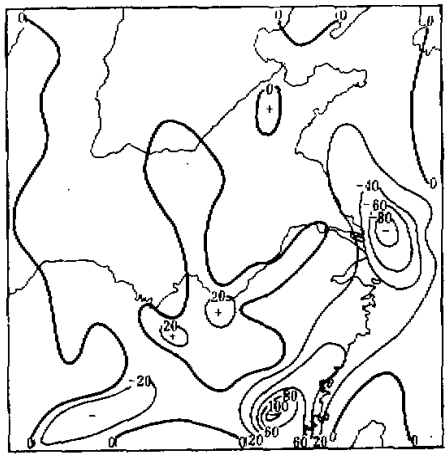

Fig. 2. Tendency of potential stability (units in 10^{-2} m²/s³) on σ=7/14 surface at 1-hr integration for Scheme 3.

centres appear in the figure. This pattern tends to persist in the process of integration. It will be shown that the mesoscale systems causing heavy rain will develop in these negative areas.

IV. ANALYSIS OF RESULTS

Integration is carried through 6 hours for all three schemes. It is seen from the variations of surface pressure that the closed circulations of lows are restored at the location of

the original Jiang-Huai Valley cyclone in each scheme after the first 1—2 hr of integration. In Scheme 1, the low is filling rapidly since there is no effect of water vapor. And in Scheme 2, in spite of the effect of observed water vapor, the low is also filling graduately for the observations are taken after the occurrence of the heaviest rainfall. Only in Scheme 3 does the low corresponding to the Jiang-Huai cyclone develop rapidly. The pressure at the low centre has fallen by about 2.5 hPa after 4-hr integration.

The flow patterns at 1000 hPa surface at 4-hr integration for Scheme 1 and 3 are shown in Fig. 3 (The result for Scheme 2 is similar to that of Scheme 1). It is seen that the simulation of Scheme 3 results in a large and nearly circular Jiang-Huai cyclone. At the 700 hPa surface there appears a strong low-level jet stream with three wind speed maxima, the strongest one being 20 m/s.

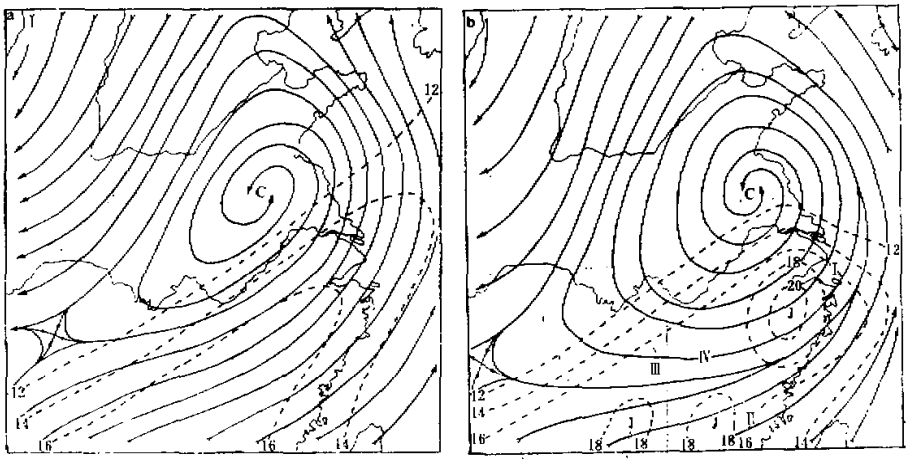

Fig. 3. Streamlines (solid) at 1000 hPa surface and isotachs (dashed, m/s) at 700 hPa surface for Scheme 1 (a) and 3 (b) at 4-hr integration. The Roman numerals in (b) are the serial number denoting centres of mesoscale systems at 4-hr integration for Scheme 3.

Little difference can be visualized intuitively between the flow fields of Schemes 1 and 3 at the 300 hPa surface at 4-hr integration (see Fig. 4). The distribution of wind speeds at the 300 hPa surface for Scheme 3, however, is quite different from that of Scheme 1 as implied by the divergence field. Three strong divergence centres are shown at the 300 hPa surface for Scheme 3. None of them coincides with the Jiang-Huai cyclone, and their horizontal extent is much smaller. The magnitudes of these divergence centres are in the order of 10^{-4}—10^{-5} s^{-1}, i.e., one order of magnitude stronger than the usual large-scale divergence. Since non-divergent initial flow is used in the simulation, the resultant strong divergence at upper level must be indications of developments of strong mesoscale systems.

In order to investigate the development of mesoscale convection within the large-scale environment and the dynamical and thermodynamical structures of the mesoscale convective systems, we use a separating operator as suggested in Ref. [7] to separate the mesoscale components from the large-scale background for the fields of surface pressure, geopotential height at the 300 hPa surface, flow field at the 1000 and 300 hPa surface, and vertical velocity at the 700 hPa surface for Scheme 3 at 4-hr integration. The results are shown in Figs. 5 and 6.

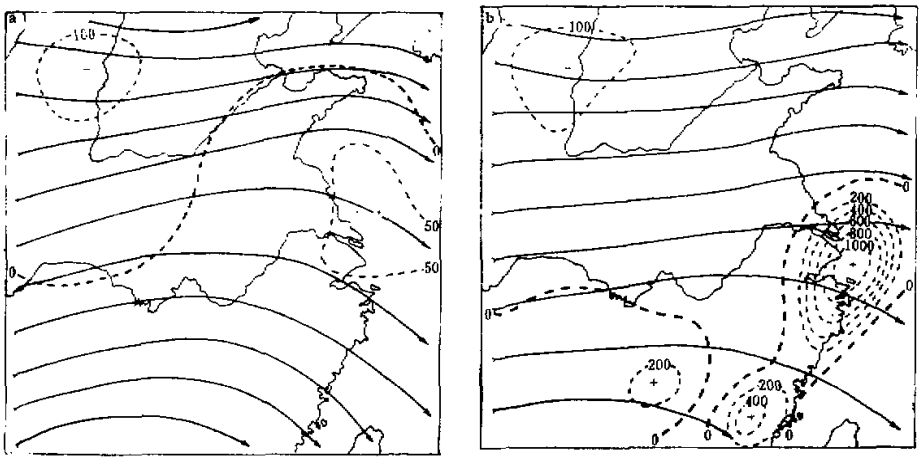

Fig. 4. Streamlines (solid) and divergence (dashed, 10^{-7} s^{-1}) at 300 hPa surface for Scheme 1 (a) and 3 (b) at 4-hr integration.

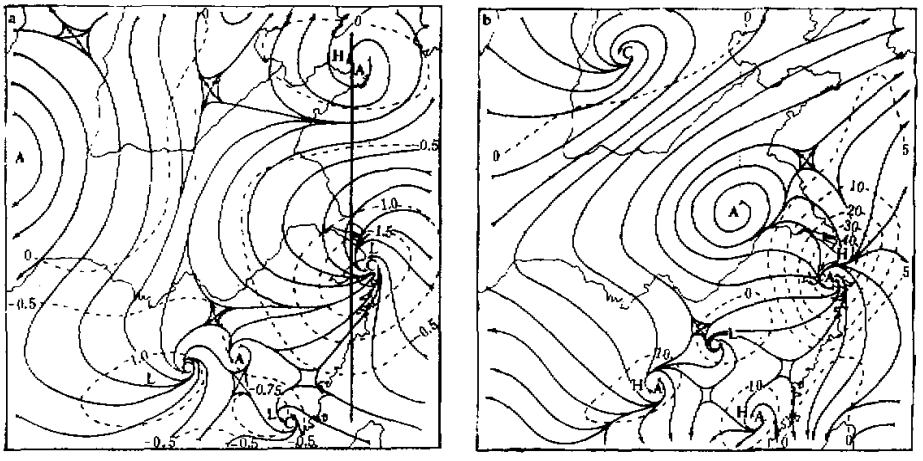

Fig. 5. Mesoscale disturbed fields for Scheme 3 at 4-hr integration.
(a) The fields of disturbed surface pressure (dashed lines, hPa) and disturbed streamlines (solid lines) at the 1000 hPa surface (The heavy straight line denotes the base line of cross section), (b) The fields of disturbed geopotential heights (dashed lines, gpm) and streamlines (solid lines) at the 300 hPa surface.

In Scheme 3, four mesoscale systems (cf. Roman numerals in Fig. 3b) are formed in the lower troposphere and located in the warm sector of the Jiang-Huai cyclone. Their horizontal spans are from 200 to 500 km. By comparison with Fig. 2, it is found that the meso-lows I, II and III are generated in the areas where the tendency of potential stability is negative, $\frac{\partial}{\partial t}\left(-\frac{\partial E_\sigma}{\partial \sigma}\right)<0$. The meso-high IV is generated in the area where the tendency of potential

stability is positive. In the field of disturbed streamlines at the 1000 hPa surface (Fig. 5a), the cyclonic flows converge towards the centres of meso-low and the anticyclonic flows diverge from the centre of meso-high to the surroundings. At the upper levels of the troposphere (Fig. 5b), the phase of disturbance at 300 hPa is opposited to that at the lower levels, i.e., upper level meso-highs are superimposed upon the lows at the surface layer, whose horizontal pressure gradients are strong and the mesoscale wind field exhibits distinct anticyclonic divergent flow. The centres of mesoscale disturbances at upper and lower levels nearly coincide, which is the characteristic feature of convective systems.

The rainfall and disturbed vertical velocity at 700 hPa for Scheme 3 at the end of the 4th-hr of integration are shown in Fig. 6. Three rainfall centres in the integration area correspond to the three meso-lows and vertical velocity maxima. Maximum rainfall is observed in mesoscale System I amounting to 47.7 mm, about two-thirds of which come from convective precipitation. System I is found to be a mesoscale convective system with vigorous convective activity and high precipitation efficiency.

Several meridional cross sections for mesoscale System I are given in Fig. 7. It is seen from Fig. 7a that there is a meso-low below 500 hPa, with maximum disturbance at the 850 hPa level, and a meso-high prevails above 500 hPa, with maximum disturbance near 200 hPa.

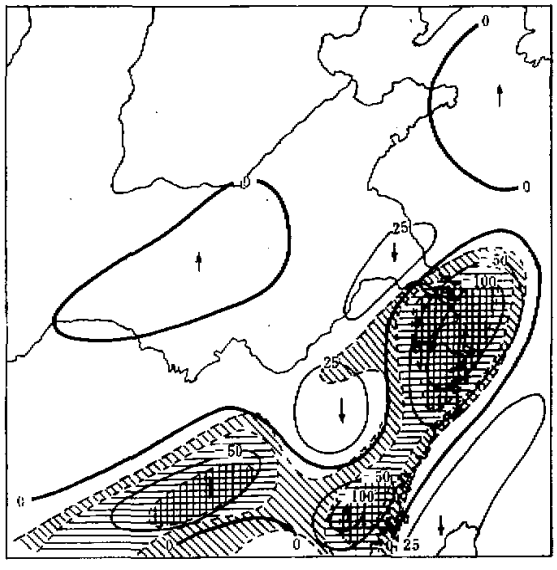

Fig. 6. Rainfall (mm) and disturbed vertical velocity (10^{-4} hPa/s) for Scheme 3 at the end of the 4th-hr of integration.
The areas of tilt, horizontal and meshed lines denote that of the amount of rainfall in 2—4, 4—15 and more than 15 mm, respectively.

A large area of increased wind speeds exists at the 200 hPa level to the north of this mesoscale high, the maximum increment being 8 m/s. Another centre of high winds appears at 700 hPa level with a maximum increment of 4 m/s to the south of the meso-low in the lower layers. This is consistent with the analysis by Maddox[2], who has analysed the composited wind field of 10 mature MCCs. This kind of distribution in disturbed wind speeds is obviously

the result of violent development of moist convection. In fact, the superimposition of the disturbed flow to the north of the meso-high on the high-level jet stream and the merging of the increased wind speeds to the southeast of the meso-low with the low-level jet stream result in a simultaneous strengthening of both the upper and lower jet streams. Uccellini[5] has pointed out that such collocation of centres of strong winds in the upper and lower jet streams is favorable for the development of mesoscale system and may cause heavy rain.

Fig. 7b is the meridional cross section of disturbed vertical currents. The mesoscale System I obtained in our simulation is a deep convective system formed in moist layers. The upward motions in the core of the meso-low prevail from the surface through the tropopause, with maximum rising velocity near 450 hPa. (The rising velocity near the base line at the 450 hPa surface amounts to -2.48×10^{-2} hPa/s.) There is organized subsidence on the periphery of this meso-low, forming the secondary vertical circulation indispensable to the

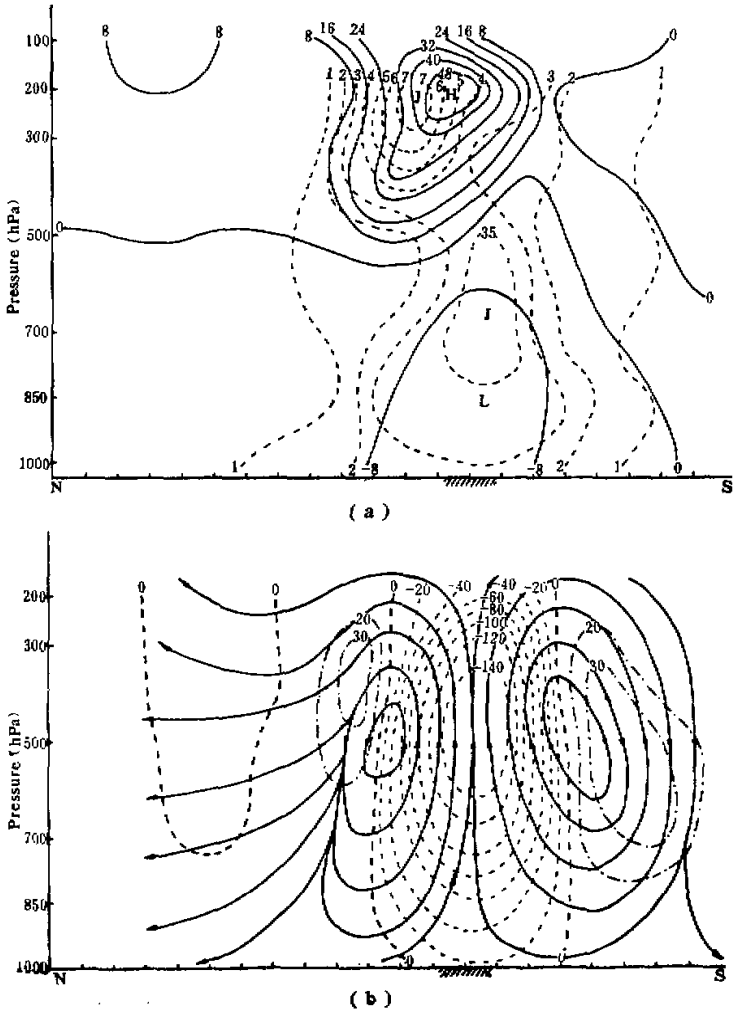

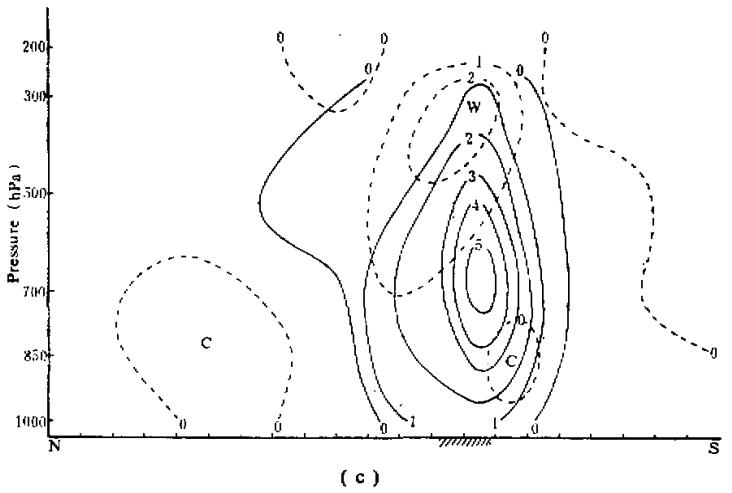

(c)

Fig. 7. Meridional cross sections of mesoscale System I (for location of base line, see Fig. 5a) for Scheme 3 at 4-hr integration.
(a) Disturbed geopotential heights (solid lines, gpm) and disturbed wind speeds (dashed lines, m/s); (b) The disturbed vertical circulation (solid lines) and vertical velocity (Dashed lines denote upward motion and dot-dashed lines denote downward motion in 10^{-4} hPa/s); (c) Heating function by condensation (solid lines, 10^4 m^2/s^2) and disturbed temperatures (dashed lines, °C). Shaded area denotes the area where the accumulated convective rainfall during 4-hr integration is larger than 40 mm.

maintance and development of mesoscale systems. The appearance of a secondary circulation not only provides better organized structure for the mesoscale system itself but also couples it with the large-scale circulation. Through this secondary circulation, the mesoscale system gets water vapor and potentially unstable energy from the large-scale environment in the lower layer, and the field of flow at the upper level is changed drastically.

Fig. 7c is the vertical cross section of heating function by condensation and disturbed temperatures. Here, the values of heating function are the accumulated release of latent heat of condensation at a point in the atmosphere in 4-hr integration. It is seen that the heating takes place mainly in the layer of potential instability below 500 hPa. The heating centre is located near 700 hPa and a magnitude as high as 5.64×10^4 m^2/s^2. Part of this great amount of energy is used to heat the ambient air through horizontal large-scale movement and a great part of it is transported to the upper troposphere by violent upward motion, to develop and strengthen the warm core structure of the mesoscale convective system. (The most intense part of the warm core is located near 350 hPa.) This heat transport also helps to maintain the strong pressure gradient between the meso-high in the upper troposphere and its environment, and the outflow mechanism, leading to the appearance of compensated downward motion and the formation and development of the secondary circulation. This kind of warm-core mesoscale convective system is similar to the MCC over the central United States. Wetzel et al.[9] and others metaphored this kind of mesoscale convective system as "heat engine" which consumes a great quantity of energy. The "heat engine" can operate continuously and even be accelerated if it obtains huge amount of water vapor and energy of potential instability from the large-scale environment. Such mesoscale

convective system has high precipitation efficiency and may persist for a longer period. With the remove of water vapor from the model atmosphere after 4-hr integration, the distribution of potential stability is changed drastically. Continuation of the integration process for 2 more hours causes the mesoscale convective systems to decay rapidly. This also proves that the potentially unstable energy is the main energy source for the maintenance and development of mesoscale systems. As soon as the source of water vapor is cut off, the potentially unstable stratification can no longer be restored rapidly, thus giving rise to a prompt decay of the mesoscale systems.

V. DISCUSSION

In our experiment, mesoscale convective systems are simulated from large-scale background. Our result further confirms the assertion that mesoscale convective systems are generated in certain special large-scale environment. This environment may exist before the presence of mesoscale convective systems.

A preliminary survey of enhanced infrared satellite images shows that the meso- or intermediate-scale cloud clusters appear frequently at the north-western side of subtropical high over the western Pacific. They are embedded in the cloud system of the warm and moist southwesterly monsoon. The cloud shapes are similar to those of the MCC except for that the horizontal extent is usually smaller than that of the latter. Some of these clusters may dissolve and disappear. Others may drift along with the southwesterlies towards the northeast and often develop violently in the south-east quarter of the Jiang-Huai cyclone and bring about heavy precipitation. The results of our simulation are in good agreement with the observed facts.

There still exist some controversial opinions as regards the nature of the MCC. Maddox[1] held that the MCC belongs to a mixed category of convective weather system which has both baroclinic and tropical features. Wetzel et al.[9], however, held that MCC is essentially a convective system of tropical nature, that is, in view of the area of genesis and structure of the simulated mesoscale convective systems in our experiment, the mesoscale convective systems developing over the Jiang-Huai Valley under moist conditions are, to a greater degree, of the nature of low-latitude convective activity. The mesoscale System II and III obtained in simulating experiment for Scheme 3 are generated in moist environment with uniform temperatures in the horizontal in the absence of westerly troughs. It is also shown by satellite photos that the mesoscale convective cloud clusters may emerge at any part of the southwesterly monsoon cloud system. However, they usually develop violently upon moving into the area ahead of a westerly trough. Both the observed facts and simulated results show that the large-scale baroclinity is not likely to be a necessary condition for the generation of mesoscale system but often acts as a trigger mechanism for mesoscale convection at middle latitudes.

The release of potential energy of instability is important for the development of mesoscale convective systems, which would develop only if the potential energy of instability could be replenished and the potentially unstable stratification be restored incessantly. In general, only a few areas can meet these conditions. According to Eq. (9) the occurrence of these conditions is decided mainly by the intricate interaction between the fields of water vapor, pressure, temperature and flow, the distribution of water vapor being most important. Therefore, the initialization of water vapor is one of the important problems to be considered in numerical prediction of heavy rainfall.

Both MCC of the central United States and the mesoscale convective system found in our simulation experiment are deep, moist convective systems which are driven by convection, possessing distinctive structure, extending over a large area and having a long-life cycle. They creat a thick convective secondary circulation which gives rise to persistent rain with high precipitation efficiency and produces a positive feedback mechanism to the large-scale environment. There is no justification, therefore, for regarding such convective system as an averaged state of isolated cumulus convections but as a weather entity existing objectively in the atmosphere. There is no comprehensive scheme of parameterization as yet to treat this kind of convective process. At present, the amount of heavy rainfall forecast by the large-scale numerical models is often much smaller than the observed value. One of the reasons may be that such convective processes are not properly incorporated in the numerical models.

In our experiment, we stress mainly the effect of water vapor on the development of mesoscale convection. In fact, the generation and development of mesoscale convective systems are the result of combined effects of various factors in the large-scale environment. And the development of mesoscale convective system, on the other hand, brings about significant influences on the large-scale environment. Particularly, the effect of large-scale flow on the generation and development of mesoscale convective system must not be neglected. Observations show that there is a close relation between the low-level jet stream and the generation and development of the MCC in the central United States and the mesoscale convective system over Southeast China. Many aspects of the related problems remain to be investigated by numerical modelling.

REFERENCES

[1] Maddox, R.A., *Bull. Amer. Met. Soc.*, **61**(1980), 11: 1374—1387.
[2] Maddox, R.A., *Mon. Wea. Rev.*, **111**(1983), 7: 1475—1493.
[3] 陶诗言等，气象学报， **41**(1983), 3: 263—274.
[4] 郑良杰等，一个用于中尺度研究的套网格 N 层原始方程模式（尚未发表）.
[5] Davies, H.C., *Quart J. Roy. Met. Soc.*, **102**(1976), 432: 405—418.
[6] Gadd, A. J., and Keers, J. F., *ibid.*, **96**(1970), 426: 297—308.
[7] 夏大庆等，大气科学， 7(1983), 3: 301—311.
[8] Uccellini, L.W., and Johnson, D.R., *Mon. Wea. Rev.*, **107**(1979), 6:682—703.
[9] Wetzel, P. J. et al., *Mon. Wea. Rev.*, **111**(1983), 10:1919—1937.